Synthesis of a new organophosphorous alkoxysilane precursor and its effect on the thermal and fire behavior of a PA66/PA6 copolymer

Jihane Sahyoun, Véronique Bounor-Legare, Laurent Ferry, R Sonnier, F da Cruz-Boisson, F. Melis, Anne Bonhommé, Philippe Cassagnau

Synthesis of a new organophosphorous alkoxysilane precursor and its effect on the thermal and fire behavior of a PA66/PA6 copolymer

J. Sahyoun [a], V. Bounor-Legaré [a,*], L. Ferry [b], R. Sonnier [b], F. Da Cruz-Boisson [c], F. Melis [a], A. Bonhommé [d], P. Cassagnau [a]

[a] Université de Lyon, Université de Lyon 1, CNRS UMR 5223, IMP, 15 Boulevard Latarjet, F-69622 Villeurbanne, France
[b] Centre des Matériaux des Mines d'Alès (C2MA), École des Mines d'Alès, 6 Avenue de Clavières, F-30319 Alès, France
[c] INSA de Lyon, IMP@INSA, UMR CNRS 5223, 20 Avenue Albert Einstein, Bat J. Verne, Villeurbanne F-69621, France
[d] Université de Lyon, Université de Lyon 1, Institut des Sciences Analytiques, UMR 5280, CNRS, ENS-Lyon, 5 Rue de la Doua, F-69100 Villeurbanne, France

A B S T R A C T

A new silicophosphorylated filler was generated *in situ* in a molten PA66 copolymer during extrusion process with the aim to improve the fire behavior of the matrix. The filler was obtained in one step via hydrolysis–condensation reactions of SiDOPO precursor (DOPO, 9,10-dihydro-9-oxa-10-phosphaphenanthrene). The synthesis of the precursor is reported and characterized by NMR. A ^{29}Si NMR study of SiDOPO hydrolysis–condensation reactions in N-methylacetamide (NMA) solvent was also conducted. Thermal stability of Cop-PA/SiDOPO composite and the major degradation products were studied by thermogravimetric analysis coupled with Infrared spectrometry (TGA/FTIR). The Pyrolysis Combustion Flow Calorimeter (PCFC) and cone calorimeter were used to investigate the fire behavior of the composite. Results show that the nanocomposite exhibits a little earlier ignition but with a decrease around 33% of the peak of heat release rate (PHRR). The presence at low concentration of silicon (0.65 wt.%) and phosphorus (0.75 wt.%) promotes the formation of an expanded char layer that acts as a barrier. A reduction of about 18% in effective heat of combustion (EHC) values suggests an additional flame inhibition effect of phosphorus in the gas phase.

Keywords:
Polyamide
Sol–gel
Fire-retardancy
DOPO-modified alkoxysilane
Reactive extrusion

1. Introduction

Nanocomposites containing organic–inorganic domains obtained through sol–gel process are nowadays widely used as an alternative to the traditional path of dispersion by blending the fillers into the polymer. Hydrolysis–condensation reactions of alkoxysilane lead to the creation of a network based on silicon. For example, silica precursors such as tetraethoxysilane (TEOS) [1] or tetramethoxysilane (TMOS) [2] have been widely used in presence of polymer [3]. In addition, several studies showed that silicon is an element that has flame retardant properties [4,5], but generally, the flame retardancy remains limited. Often, the latter is introduced in the presence of other functions such as phosphorus flame retardant groups. Several authors have already examined the phosphorus functionalization of silica, for enhancing the fire retardancy of polymers [6,7]. The use of diethylphosphatoethyltriethoxysilane (SiP) as silicophosphorated precursor was reported to be a good flame retardant for hybrid compositions due to the synergistic effect Si—P. For example, Chiang and Ma [6] grafted

* Corresponding author.
E-mail address: bounor@univ-lyon1.fr (V. Bounor-Legaré).

alkoxysilane coupling agent on an epoxy resin in order to form covalent bonds between the matrix and the inorganic phase synthesized from TEOS and SiP. The values of the limiting oxygen index (LOI) were increased from 24% to 32% in the presence of the inorganic network. Alongi et al. [7] used the diethylphosphatoethyltriethoxysilane for preparing a phosphorus–silicate hybrid structure, by hydrolysis–condensation reactions, in order to increase the thermal stability and the fire properties of cotton. The cotton fabrics were impregnated with the hybrid sols. Two series of treated fabrics characterized by a different layer number consisting of 1–6 consecutive depositions were prepared with or without condensation catalyst (dibutyl tindiacetate, DBTA). Results showed that the presence of the coating decreased the cellulose decomposition temperature but, at the same time increased the amount of the residue. The flammability data showed that the hybrids prepared without DBTA have been able to enhance the total burning time and to form the highest residues after the test. But the time to ignition (TTI) was decreased in the presence of 3 or 6 layers; this was consistent with observations in TGA under air. Despite the reduction in TTI, the hybrid coatings were found to protect the cotton fabrics by reducing significantly the duration of the combustion and inhibiting the formation of volatile species. Concerning thermoplastic resins such as polyamide 6 (PA6), Theil-Van Nieuwenhuyse et al. [8] studied the *in situ* generation of phosphorylated silica by sol–gel method within a PA6 matrix in the molten state during extrusion and its influence on the polymer fire behavior. Results have shown a significant decrease about 50% of the peak of heat of release rate and the formation of an important residue during cone calorimeter test with the addition of only 2.5 wt.% of silicon and 2.5 wt.% of phosphorus. Secondly, HRR curves were modified from pure PA6 to SiP based nanocomposites evidencing a change in the PA6 fire behavior from non charring materials to thermally thick charring materials. However, the ignition of the SiP based composite occurred earlier than the PA6. This tendency was also observed in thermogravimetric analysis under air and was attributed to the catalytic effect of phosphorus compounds and was more pronounced with the SiP based nanocomposites [9]. This decrease of the time to ignition was also observed for ethylene vinyl acetate EVA/SiP based composites [10]. This paper focuses on the functionalization of silica with a different phosphorylated group, by substituting the structure of the phosphorus group of SiP with a more stable structure such as 9,10-dihydro-9-oxa-10-phosphaphenanthrene (DOPO) in order to try to overcome the only problem, which is the early ignition of the SiP based composites. DOPO group is a monofunctional phosphinate that shows a high reactivity toward the double C═C bond [11], high thermal stability and good water resistance. DOPO and its derivatives have been widely used for improving the flame retardancy of epoxy resins [12–14].

Zhang and Yang [15] reported a new approach to the synthesis of phosphorus-containing polyhedral oligomeric silsesquioxanes (POSS). The reactions are first based on the addition reaction between the P—H group of DOPO and the C═C bond of vinyl triethoxysilane (VTES) and then on hydrolysis-condensation reactions of the DOPO–VTES in order to obtain DOPO–POSS that showed superior thermal stability comparing to common polymeric materials. Concerning the fire behavior, Alongi and Malucelli [16] used TMOS as an inorganic precursor of the silica phase coupled with DOPO as a flame retardant. The deposited coating on the cotton fabric favored the char formation and hindered the evolution of volatile species. The most interesting observation was that the time to ignition value was not affected by the presence of the deposited coating CO–Si–DOPO (CO for cotton fabrics). Hu et al. [17] synthesized poly(DOPO–VTES) for polycarbonate (PC). The T_{onset} (defined as the temperature at which 5% weight loss occurs) and the residue under nitrogen atmosphere increased with the addition of 5 wt.% of poly(DOPO–VTES), which is associated with the good thermal stability of poly(DOPO–VTES). LOI values increased with the poly(DOPO–VTES) contents from 24.3% to 32.8% with PC/5 wt.% P(DOPO–VTES). In another work, Wei et al. [18] studied the co-condensation of VTES and TEOS in the presence of poly(ethyleneglycol)-B-poly(propyleneglycol)-B-poly(ethyleneglycol) (P123) surfactants followed by DOPO modification for enhancing the fire retardancy of polycarbonate/acrylonitrile–butadiene–styrene (PC/ABS). Results showed that the addition of 2 wt.% of DOPO-grafted hybrid mesoporous silica (DM) in PC/ABS increased the LOI values from 23% to 25%. A little reduction (5 °C) of the T_{onset} was also observed under nitrogen atmosphere, which did not change the thermal degradation process. Concerning the fire performance, a reduction about 10% of the heat release rate was observed with the addition of 2 wt.% of DM. Furthermore, the TTI was slightly increased from 50 to 55 s. Lately, Qian et al. [19] prepared novel organic/inorganic epoxy hybrids containing DOPO and silica synthesized by *in situ* polymerization. The sol–gel and thermocuring processes were employed to incorporate the DOPO–VTS (vinyltrimethoxysilane) into the structure of epoxy resins. The LOI of the epoxy/DOPO–VTS hybrids increased from 22.5% to 32% and the hybrids containing 15 wt.% of DOPO–VTS can reach V-0 rate in UL94 vertical test.

These observations on the relatively good thermal stability of SiDOPO are very encouraging. Thereby, the aim of this paper is to study the influence of the new precursor called SiDOPO from VTES and DOPO on the thermal and fire behavior of a PA66 copolymer. In first step, we report the synthesis and the NMR characterization of the SiDOPO precursor. A ^{29}Si NMR study of SiDOPO hydrolysis–condensation reactions in N-methylacetamide (NMA) solvent is also conducted. Afterwards, the precursor is injected in the molten copolymer during the extrusion process. The phosphorylated silica filler is generated *in situ* via hydrolysis–condensation reactions during melt extrusion in one step without adding solvents.

Furthermore, the thermal properties and the major degradation products of the prepared composite are studied. Fire performances are based on pyrolysis combustion flow calorimeter and cone calorimeter tests.

2. Experimental

2.1. Materials

PA66/PA6 (90:10 wt.%) copolymer denoted Cop-PA was kindly provided by Solvay group under the trade name STABAMID 25 RS 5 S2 for spinning applications. Vinyl triethoxysilane (VTES, $\geqslant$98%) and azobisisobutyronitrile (AIBN, 98%) were purchased from Sigma–Aldrich (France). 9,10-Dihydro-9-oxa-10-phosphaphenanthrene (DOPO) was obtained from ABCR Gelest (Germany). Tetrahydrofuran (THF, anhydrous) was purchased from Carlo Erba Reagents (France). All materials were used without further purification.

2.2. Synthesis of SiDOPO

The synthesis of the organophosphorous alkoxysilane precursor was conducted according to the following procedure with a molar ratio of DOPO:VTES:AIBN of 1:1.5:0.05. First of all, 5 g (0.0231 mol) of DOPO were added to a round bottom two-necked flask with a magnetic stirrer and a reflux condenser under nitrogen atmosphere at 80 °C. The product was dried for several minutes before adding 25 mL of THF. After solubilization, 6.6 g (0.0346 mol) of VTES were introduced and the solution was stirred for 15 min. Finally, 0.19 g (0.0012 mol) of AIBN were slowly added to the solution. The temperature was held at 80 °C for 10 h. The obtained light yellow liquid precursor was purified by rotary evaporation at 160 °C in order to remove any excess of solvent or VTES.

2.3. Composite preparation

Cop-PA pellets were dried 48 h at 80 °C under vacuum prior to use. The composite was prepared by melt blending in a corotating twin screw extruder (Leistriz LSM model, diameter 30 mm, L/D 34) operating at 250 °C. The pellet feed rate was set at 3 kg/h with a screw rotation speed of about 150 rpm. The SiDOPO precursor was added into the matrix in the molten state at a constant flow rate using an external liquid pump. The prepared composite is shown in Table 1.

For the cone calorimeter test, the extrudates were granulated into pellets. The extruded pellets were dried 24 h at 80 °C under vacuum and then injection-molded at about 270 °C to prepare specimens with dimensions of about $(100 \times 100 \times 4)\,mm^3$. The injection molding machine is a Krauss Maffei, (KM50/180CX model) characterized by a screw diameter of 28 mm and a ratio L/D = 25.

Table 1
Composition of the SiDOPO composite prepared through the extrusion process.

Materials	SiDOPO content (calculated wt.%)	Measured wt.% of Si[a]	Measured wt.% of P[a]	Ratio P/Si
C10SiDOPO	10	0.65	0.75	1.15

[a] Determined by elemental analysis.

2.4. Measurements

2.4.1. NMR study

The synthesized SiDOPO precursor was characterized by ^{1}H, ^{29}Si and ^{31}P NMR in deuterated chloroform ($CDCl_3$). Spectra were recorded with a 5 mm BBFO + probe on a Bruker AVANCE III spectrometer operating at 400.1 MHz for ^{1}H, 79.5 MHz for ^{29}Si and 162.0 MHz for ^{31}P. Chemical shifts values are given in ppm according to internal tetramethylsilane (TMS) standard.

To follow the hydrolysis–condensations conversions, the reactions were studied in alkoxysilane/NMA/deionized water systems. The N-methylacetamide (NMA) was used as a model medium because its structure comprises the repeating unit of the polyamide chain. The lock signal was provided with an internal coaxial tube of DMSO-d6. ^{29}Si NMR spectra were obtained at 79.5 MHz on a Bruker AVANCE II spectrometer with a 10 mm selective ^{29}Si probe. Hexamethyldisilane was used as an additional calibration substance since its signal remains constant throughout the experiment. Chromium acetylacetonate $Cr(acac)_3$ was added to shorten the ^{29}Si spin–lattice relaxation times. Experiments were carried out at 30 °C. Spectra were recorded with inverse gated proton decoupling, a 70° pulse angle and 11 s recycling time to allow a quantitative analysis. 128 scans were recorded for each spectrum. Uncertainty of the measurements was estimated to be ±5%. The reaction times were determined by the initial time of the measurements even though some evolution may occur during acquisitions especially if the hydrolysis–condensation reactions occur rapidly.

The reaction mixture was prepared by introducing first the organophosphorous alkoxysilane precursor in a 10 mm tube. Then NMA, HMDS and $Cr(acac)_3$ were added (Silane/NMA/HMDS/$Cr(acac)_3$ molar ratio: 1/20/0.1/0.03). The mixture was stirred and the first recorded spectrum is t_0. Finally, the beginning of the kinetics is indicated by the addition of water which initiates the hydrolysis reaction then the first spectrum recorded after the addition of the water is t_1 (Silane/NMA/water molar ratio: 1/20/5).

^{29}Si solid state NMR was performed using a Bruker ADVANCE 500 spectrometer with a Bruker 4 mm CPMAS (cross-polarization magic angle rotation) probe. The ^{29}Si spectrum was recorded at 99.36 MHz. The sample rotation speed was at 5 kHz. The samples were analyzed as finely ground powder.

In the literature [20], classical notation is T for silicon containing three oxygen bridging atoms. This notation is completed by i and j indices (T^{ij} i,j = 0, 1, 2 or 3) where i is the number of oxo Si—O—Si bonds and j is the number of hydroxy functions.

2.4.2. Characterization of thermal decomposition

Thermogravimetric experiments were performed using a SDT Q600 TGA from TA Instruments. The samples were heated in open alumina pans from room temperature up to about 750 °C at a heating rate of 10 °C/min under nitrogen or synthetic air flow of 25 mL/min. Reported data are T_{onset} at which the formulation displays 5 wt.% weight loss, T_m at which the decomposition rate is the highest and the amount of residue at 700 °C.

TG coupled Infrared spectroscopy was conducted in order to identify evolved decomposition products. For this purpose a Q50 thermogravimetric analyzer (TA Instruments) was coupled to a Nicolet Nexus spectrometer with an MCT detector. The temperatures of the transfer line and the gas cell were maintained at 240 °C. The infrared spectrometer was operated at an optical resolution of 4 cm^{-1}. Experiments were performed under nitrogen or air with a gas flow rate of 90 mL/min. The samples (about 10 mg) were heated in open alumina pans, from 30 °C up to about 700 °C at a heating rate of 5 °C/min. Components identification was based on characteristic peaks and by subtraction of recognizable products (such as water), evolution profiles were also plotted in terms of time or temperature.

Pyrolysis Combustion Flow Calorimeter (PCFC) analyses were performed on a Fire Testing Technology (FTT) apparatus. Samples around 2–3 mg were heated from 85 °C up to 750 °C at a heating rate of 1 °C/s under nitrogen flow. The degradation products are then collected in a second chamber (combustor) maintained at 900 °C in the presence of oxygen (N_2/O_2 mixture 80/20). In this second chamber and at this temperature, the complete combustion of the pyrolysis gases takes place. Reported values such as heat release rate (HRR), peak of heat release rate (PHRR) are measured as a function of temperature of pyrolysis. The HRR value is calculated from oxygen consumption according to the principle of Huggett [21], which explains that for organic compounds, the heat of combustion is proportional to the amount of oxygen required for combustion; i.e. 13.1 kJ/g of oxygen consumed. The heat release capacity (HRC) is calculated as the ratio of PHRR/heating rate. HRC is an intrinsic flammability parameter of a material which is supposed to be a good predictor of the larger scale fire behavior, it has been proposed as the single best measure of the fire hazard of a material [22]. The uncertainties in measurements for the apparatus are about 5%.

The ratio between the total heat release (measured in PCFC) and the mass loss (measured in thermogravimetric analysis) allows calculating the effective heat of complete combustion (called EHC_{PCFC}). Combustion efficiency in cone calorimeter is then calculated as the ratio between the EHC in cone calorimeter (EHC_{cone}) and EHC_{PCFC}.

2.4.3. Characterization of fire behavior

The combustion behavior of materials was investigated using a cone calorimeter (CC) supplied by FTT company. Experiments were carried out at an irradiance of 50 kW/m^2 according to ISO 5660 standard. The distance between the cone heater and the sample was 25 mm. Time to ignition (TTI, s), time to flame out (TTF, s), total heat release (THR, MJ/m^2), peak of heat release rate (PHRR, kW/m^2), effective heat of combustion (EHC, kJ/g), and the percentage of the residue (%) were measured. The value of HRR is also calculated from the oxygen consumption according to the principle of Huggett [21]. To ensure significant and reproducible data, experiments were repeated four times. The uncertainties in measurements for the apparatus are about 15%.

2.4.4. Morphology study

The morphological study of the composite and of the residual layer formed during sample degradation in cone calorimeter test was performed using a scanning electron microscope FEI Quanta 200 SEM equipped with an energy dispersive X-ray (EDX) spectrometer. Images were obtained under high vacuum at a voltage of 12.5 kV. For samples preparation, composites are placed in liquid nitrogen for a few minutes before the cryofracture. The samples are then coated with a thin layer of carbon prior to using in the SEM to prevent charging under the electron beam, while the residue is stuck to a sample holder with a thin silver layer.

2.4.5. Elemental analysis

Elemental analysis was conducted at the Institut des Sciences Analytiques (ISA, CNRS). Silicon and Phosphorus contents were determined by ICP-AES (inductively coupled plasma-atomic emission spectrometer). The sample was in the form of a fine ground powder.

3. Results and discussion

3.1. NMR characterization of SiDOPO

^1H NMR spectrum of SiDOPO precursor is shown in Fig. 1. The emergence of the following chemical shifts: 0.68–0.85 ppm and 1.98–2.06 ppm corresponding to Si—CH_2 and P—CH_2 methylene protons respectively, evidenced that organophosphorous alkoxysilane precursor has been successfully synthesized. The split of methyl (A and A′) [15] and methylene (B and B′) signals were probably due to the partial formation of SiDOPO dimer. We found that the minor proton signal around 3.8 ppm belongs to unidentified ethoxysilane groups of a different structure than SiDOPO. The signal at 8.74 ppm was found to be one half of the doublet assigned to the proton P—H [23] of unreacted DOPO. No significant peaks for Si—CH=CH_2 protons corresponding to unreacted VTES were observed (5.9–6.1 ppm).

Furthermore the ^{31}P spectrum (Fig. 2) showed two main signals at 14.69 and 39.65 ppm assigned to the unreacted phosphorous of DOPO and linked phosphorous in SiDOPO respectively. From ^1H NMR spectrum, the amount of unreacted DOPO was about 13 mol.%. ^{29}Si NMR (in $CDCl_3$, not shown here) characteristic signal of the pure SiDOPO was a doublet at −47.9 ppm with a coupling constant $J_{Si—P}$ = 36 Hz which characterization is relatively similar to the one observed for diethylphosphatoethyltriethoxysilane (SiP) precursor in the literature [24,25].

3.2. ^{29}Si NMR study of SiDOPO hydrolysis–condensation reactions in NMA solvent

The reaction mixture SiDOPO/NMA/HMDS/$Cr(acac)_3$ was first analyzed. A zoom of the ^{29}Si NMR spectrum before the addition of water is shown in Fig. 3. The singlet at −20.1 ppm assigned to silicon from HMDS was not shown here. Two doublets were observed at −48.3 and −46.1 ppm corresponding to SiDOPO

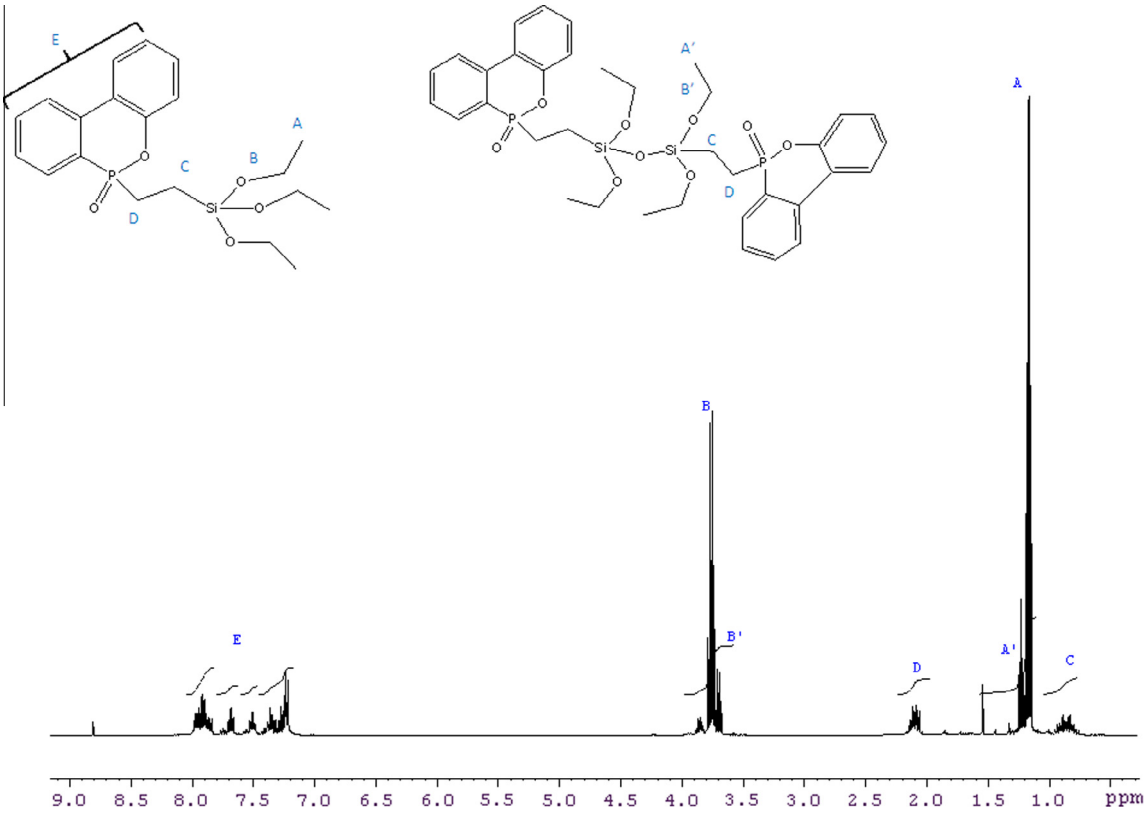

Fig. 1. ^{1}H NMR spectrum ($CDCl_3$, 27 °C) of SiDOPO precursor.

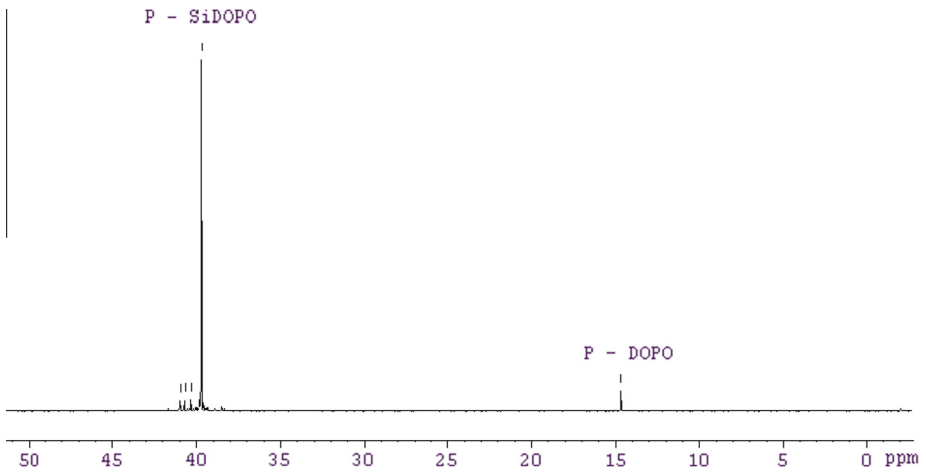

Fig. 2. ^{31}P NMR spectrum ($CDCl_3$, 27 °C) of SiDOPO precursor.

monomer (T^{00}) and its first hydrolyzed species (T^{01}) respectively. The signals were slightly shielded (about 0.4 ppm) compared to those observed in $CDCl_3$, due to the presence of NMA.

Small signals were observed around −45.7, −46.8 and −55 ppm. These signals were not attributed; they are probably due to the formation of side products from the synthesis of SiDOPO. Moreover, the doublet around −55 ppm was not attributed to condensed species since the coupling constant was in the order of 46 Hz.

Fig. 4 shows a comparison of the observed signals in NMA at different reaction times after the addition of water (SiDOPO/water: 1/5). After 1 h 14 min (1), the signals observed at −48.3 and −46.1 ppm disappeared and four new doublets centered at −43.5, −51.5, −51.8 and −60.5 ppm appeared indicating that the monomer was

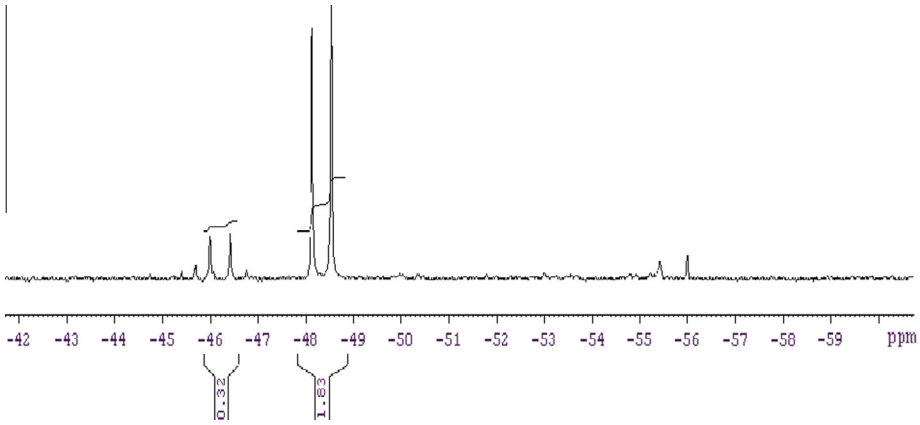

Fig. 3. ^{29}Si NMR spectrum (NMA, 27 °C) of SiDOPO before addition of water.

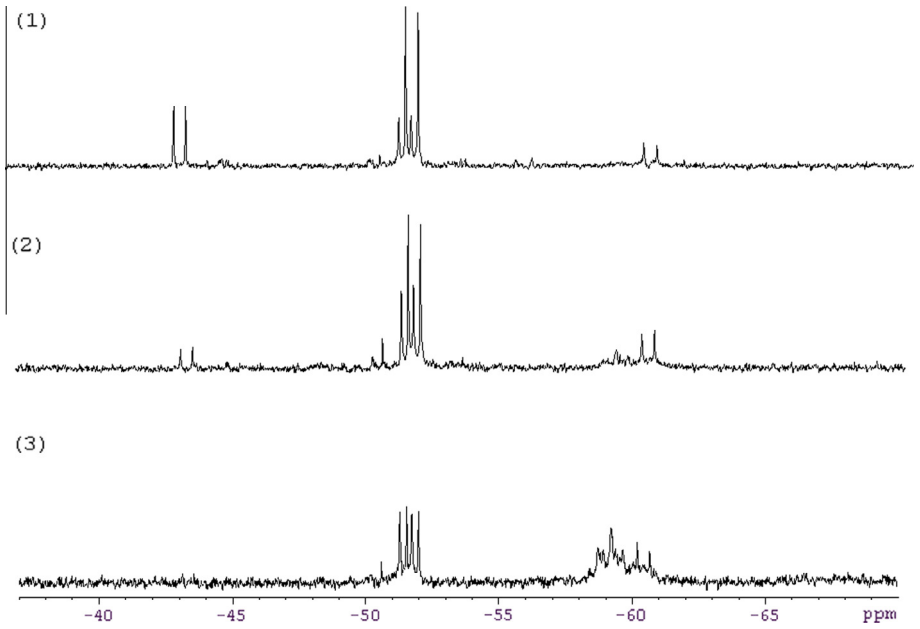

Fig. 4. ^{29}Si NMR spectra of SiDOPO in NMA at 30 °C after 1 h 14 min (1), 3 h 44 min (2), and 12 h 9 min (3) of reaction (SiDOPO/NMA/water molar ratio: 1/20/5).

completely transformed to hydrolyzed and condensed species. The first doublet at −43.5 ppm was assigned to the second (T^{02}) hydrolyzed species. No spectral signature was observed for the third (T^{03}) hydrolyzed species.

The signal at −51.8 ppm was assigned to $T^{12}T^{12}$ dimer as it did not seem to be in relation with any other signal. Furthermore, the doublet at −60.5 ppm in the T^2 region and the other additional doublet at −51.5 ppm appeared at the same time during the reaction with a constant intensity ratio of 2, evidencing their assignment to T^{21} and T^{12} species respectively in the trimer $T^{12}T^{21}T^{12}$.

After 3 h 44 min of reaction (2), the T^{02} signal was still present but with a decreased intensity and after 12 h 09 min (3), it was totally disappeared. The main signals were then observed around −60 ppm corresponding to T^{2j} species. Their multiplicity and overlapping made their individual identification very difficult. For the longest reaction times, we also observed the appearance of condensed products with T^3 units that give a broad signal centered at −67 ppm.

Although the signals from SiDOPO got broader as the reaction proceeds, by comparing their integrals with the one from internal HMDS standard, we found no significant loss of silicon by precipitation of condensed species.

A summary of the assignments of ^{29}Si NMR signals are given in Table 2.

The hydrolysis and condensation reactions of the SiDOPO precursor performed with a weak concentration of precursor (molar ratio = 1/20) allowed to evidence the influence of the amide group on the reaction rates. The reactions in a model medium (N-methylacetamide) at 30 °C showed that after approximately 1 h, the whole

Table 2
Assignment of ^{29}Si NMR signals observed during hydrolysis–condensation reactions of SiDOPO in NMA solvent.

Chemical shift (ppm)	Assignment	Formula
−48.3	T^{00}	$RSi(OEt)_3$
−46.1	T^{01}	$RSi(OH)(OEt)_2$
−43.5	T^{02}	$RSi(OH)_2(OEt)$
−51.5	$T^{12}T^{21}T^{12}$	$R(OH)_2SiOSi(OH)(R)OSi(OH)_2R$
−51.8	$T^{12}T^{12}$	$R(OH)_2SiOSi(OH)_2(R)$
−60.5	$T^{12}T^{21}T^{12}$	$R(OH)_2SiOSi(OH)(R)OSi(OH)_2R$
−58 to −61.2	All T^{2j} species	
−64 to −71	All T^{3j} species	

amount of the monomer was converted into hydrolyzed and condensed species.

3.3. Structural characterization of the phosphorylated silica/Cop-PA nanocomposite by solid NMR

The extent of the condensation reactions was estimated from the ^{29}Si CP-MAS NMR spectrum recorded on the materials obtained directly at the die of the extruder. On the spectrum of Fig. 5 we observe the emergence of four signals. The two peaks around −47 and −51 ppm were attributed to the small amount of unreacted monomer and condensed T^1 species respectively. The chemical shifts around −58 and −68 were attributed to the condensed T^2 and T^3 species of SiDOPO respectively. These results show clearly that the hydrolysis–condensation reactions occurred for the SiDOPO precursor during the Cop-PA extrusion process with the formation of highly condensed species T^2 and T^3.

3.4. Composite morphology

The composite morphology is shown in Fig. 6. On these pictures, we can see the presence of spherical particles homogeneously dispersed in the polymer matrix. However, the size distribution of the spherical particles is broad, from 170 to 460 nm with the presence of larger aggregates (around 700–790 nm).

3.5. Thermal decomposition

3.5.1. Thermal stability and residue

3.5.1.1. Thermal degradation under inert atmosphere. TG and DTG curves for Cop-PA and C10SiDOPO under helium are shown in Fig. 7. The TG curve for the pure copolymer showed a minor weight loss (<1 wt.%) between 100 and 200 °C corresponding to the residual water in the samples. One major degradation step occurred with an onset decomposition temperature of 394 °C and a T_m at 440 °C, leaving a residue of about 2 wt.% at 700 °C.

The C10SiDOPO composite exhibited a somewhat lower onset decomposition temperature around 363 °C and a much higher amount of residue (6.9 wt.%) than the neat Cop-PA, which is associated with the good thermal stability of the silico-phosphorylated filler generated *in situ* in the molten copolymer. Precisely, a minor mass loss was also observed between 200 and 250 °C corresponding to the residual water and ethanol released due to further hydrolysis–condensation reactions or trapped in the polymer matrix. However, one major degradation step occurred with a T_m at 428 °C. Table 3 summarizes thermogravimetric analysis results under helium and air.

3.5.1.2. Thermal degradation under air. Fig. 8 shows the TG and DTG curves for Cop-PA and C10SiDOPO under air. The copolymer undergoes two main degradation steps. The first important degradation step occurs between 350 and 480 °C with an onset degradation temperature of about 389 °C. The second decomposition step appears between 480 and 600 °C. This thermal degradation behavior of polyamides, under air, was described in the literature [26] by the formation of a carbonaceous layer that remains stable until 500 °C and then decomposes at higher temperatures.

However, the thermal degradation of the SiDOPO based composite under air consists of two main degradation steps whose maximum rates are found at 416 °C and

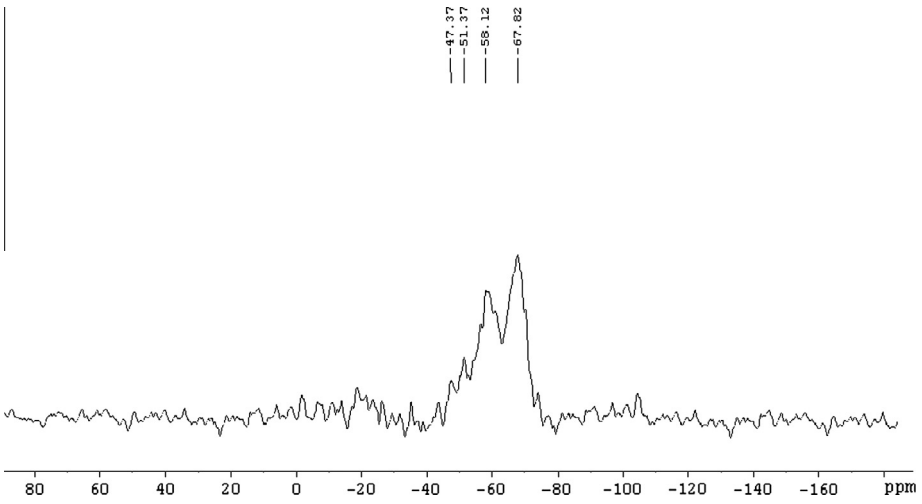

Fig. 5. ^{29}Si CP-MAS NMR spectrum of Cop-PA + SiDOPO.

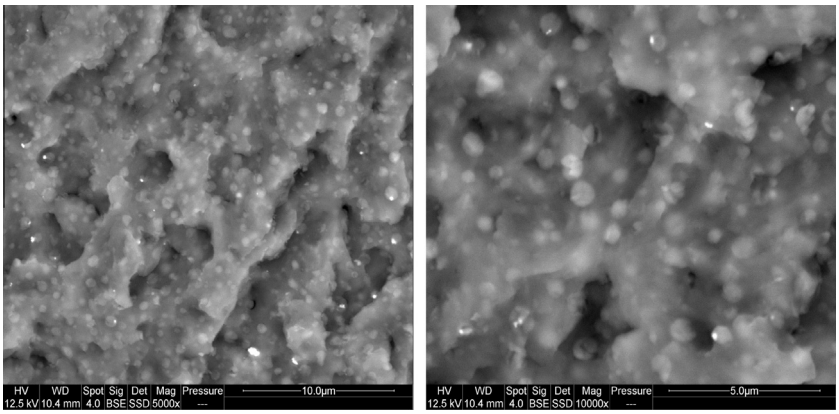

Fig. 6. SEM images of C10SiDOPO composite.

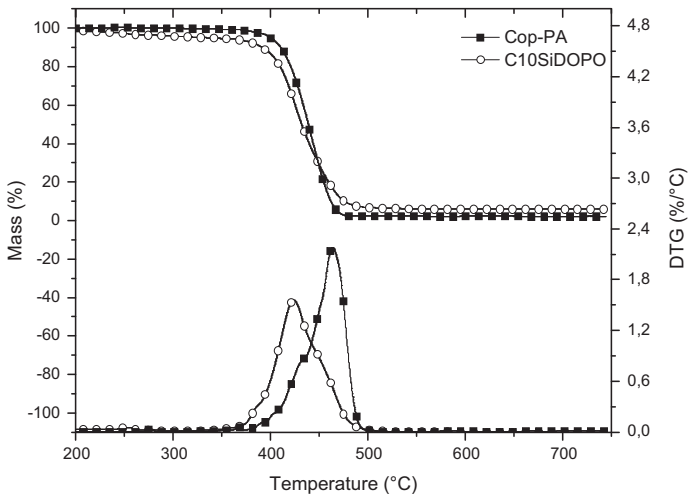

Fig. 7. TG and DTG curves of Cop-PA and C10SiDOPO composite under helium (heating rate 10 °C/min).

Table 3
Thermogravimetric analysis results under helium and air.

Sample	Cop-PA (He)	C10SiDOPO (He)	Cop-PA (air)	C10SiDOPO (air)
T_{onset} (°C)	394	363	389	346
T_m (°C)	460	428	448	416–461[a]
Residue (wt.%)	2.0	6.9	1.1	5.5

[a] Second peak.

461 °C respectively, plus the final weight loss about 11.9 wt.% between 494 and 700 °C. In greater detail, the former corresponds to a significant weight loss about 44 wt.% occurring in a range of temperature between 346 and 436 °C and the latter is of 32.6 wt.% between 436 and 494 °C, with a final residue of 5.5 wt.% at 700 °C. The main difference observed concerns the first step of degradation, which takes place at temperatures lower than for the Cop-PA.

3.5.2. Evolved gas analysis

3.5.2.1. TGA-FTIR results of Cop-PA and C10SiDOPO composite. Under inert atmosphere, the Cop-PA displays one mass loss between 350 and 480 °C. In this range of temperature, infrared analysis shows the emission of the following gases: carbon dioxide, ammonia, water vapor, hydrocarbons, as well as various carbonyl compounds. From 440 up to 500 °C, a band at 1666 cm^{-1} assigned to an amide carbonyl is observed. Another carbonyl vibration at 1766 cm^{-1} between 350 and 465 °C was attributed to cyclopentanone [27,28]. Finally, another carbonyl band located at 1702 cm^{-1} is observed between 395 and 480 °C also assigned to an amide carbonyl. Methane (CH_4) was also released around 480 °C.

Under air, the Cop-PA displays two mass losses. The first mass loss occurs from 300 to 470 °C, followed by the second one from 470 to 700 °C. Analysis showed the emission of the same gases found under inert atmosphere, except for carbon monoxide, isocyanic acid, hydrogen cyanide and some aliphatic ketones with maximum emission intensity around 440 and 455 °C. Aldehydes like acetaldehyde appear between 380 and 470 °C.

For C10SiDOPO, surprisingly, under inert atmosphere with a heating rate of 5 °C/min, the degradation occurs in two main steps this time, instead of one step. This

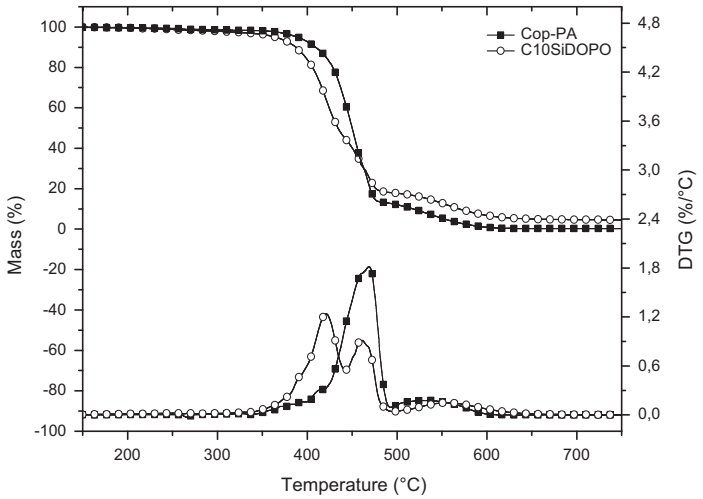

Fig. 8. TG and DTG curves of Cop-PA and C10SiDOPO composite under air (heating rate 10 °C/min).

difference is probably related to the different heating rate (5 °C/min instead of 10 °C/min). A first minor loss about 6.5 wt.% takes place between room temperature and 300 °C, followed by a significant weight loss about 52 wt.% in a range of temperature between 300 and 430 °C and the latter is of 33 wt.% between 430 and 510 °C, with a final residue of 8 wt.% at 700 °C.

Infrared analysis showed the emission of various volatile products. The evolution profile of some detected gases was plotted as a function of time (Figs. 9 and 10). Water vapor was found between 75 and 200 °C corresponding to the residual water in the sample and then reappeared between 320 and 440 °C with maximum emission intensity around 405 °C, regarded as a volatile of the polyamide degradation or polycondensation of some silanols. Ethanol was detected in a range of temperature between 95 and 280 °C. Ethanol trapped on the surface of the sample is released around 100 °C. At higher temperatures the amount released is likely due to ethanol trapped in the core of the sample and might probably be related to a new amount of ethanol produced during further hydrolysis–condensation reaction of unreacted SiDOPO, or further condensation reaction of some silanols with alkoxy silanes groups. The major volatiles were carbon dioxide between 300 and 440 °C, and ammonia between 330 and 450 °C. The maximum emission intensity for both gases was around 400 °C. The analysis showed also the presence of ethylene (low intensity) between 425 and 490 °C. Different types of aromatic groups seem to appear around 420 °C. Two carbonyl vibrations around 1706 cm^{-1} and 1769 cm^{-1} were observed in a range of temperature between 370 and 430 °C, corresponding probably to an aliphatic ketone and cyclopentanone (major degradation product of PA66) respectively. Another carbonyl vibration at 1665 cm^{-1} related to an amide function appears from 400 °C till the end of the test with maximum emission intensity around 400 °C. Compounds having alkyl chains have also been detected between 370 and 500 °C.

The TGA thermogram for C10SiDOPO under air showed four mass losses. A minor mass loss about 6.3 wt.% is observed from room temperature to 300 °C, followed by two significant weight losses of 42 wt.% between 300 and 425 °C and 32.6 wt.% between 425 and 480 °C. The final mass loss from 480 °C till the end of the test was about 12.4 wt.% yielding a final residue of 6.6 wt.%.

Under air, the emission of carbon monoxide was found between 415 °C till the end of the test. Isocyanic acid was detected in a range of temperature between 350 up to about 470 °C. The analysis revealed also the emission of methane with maximum emission intensity around 460 °C and hydrogen cyanide between 420 and 490 °C.

Except for these gases, infrared analysis showed the emission of the same gases found under inert atmosphere. Some differences were observed in the maximum emission intensities for some gases; for example, two maxima were detected for water vapor around 400 and 450 °C. Similarly, carbon dioxide released from 165 °C till the end of the test, had two emission maxima at 395 and 540 °C. Compounds having alkyl chains have also been detected between 350 and 500 °C. Between 220 and 425 °C, a carbonyl vibration at 1715 cm^{-1} was observed; this band is consistent with ε-caprolactam (major degradation product of PA6) corresponding to the little fraction of PA6 (10 wt.%) in the PA66 copolymer matrix. The characteristic band of cyclopentanone was not observed; leading us to consider that, under air, cyclopentanone probably undergoes several decompositions into products of lower molar mass or may react with other products by cross-linking [29]. Different types of aromatic groups and an alcohol function seem to appear around 420 °C, corresponding probably to phenols. Fig. 11 shows histograms for different gases as a function of temperature for Cop-PA and C10SiDOPO under both, air and nitrogen atmospheres.

Under both atmospheres, few vibration bands may indicate the presence of phosphorous compounds such as P═O (1232 cm^{-1}) [30,31]. Another band at 1118 cm^{-1} may probably be attributed to P—O—C_{arom} [31,32]. A band was also observed at 1062 cm^{-1} and may be attributed to P—O—C vibration [33]. The broad bands at 1062, 1118 and 1159 cm^{-1} may also be attributed to Si—O—C and

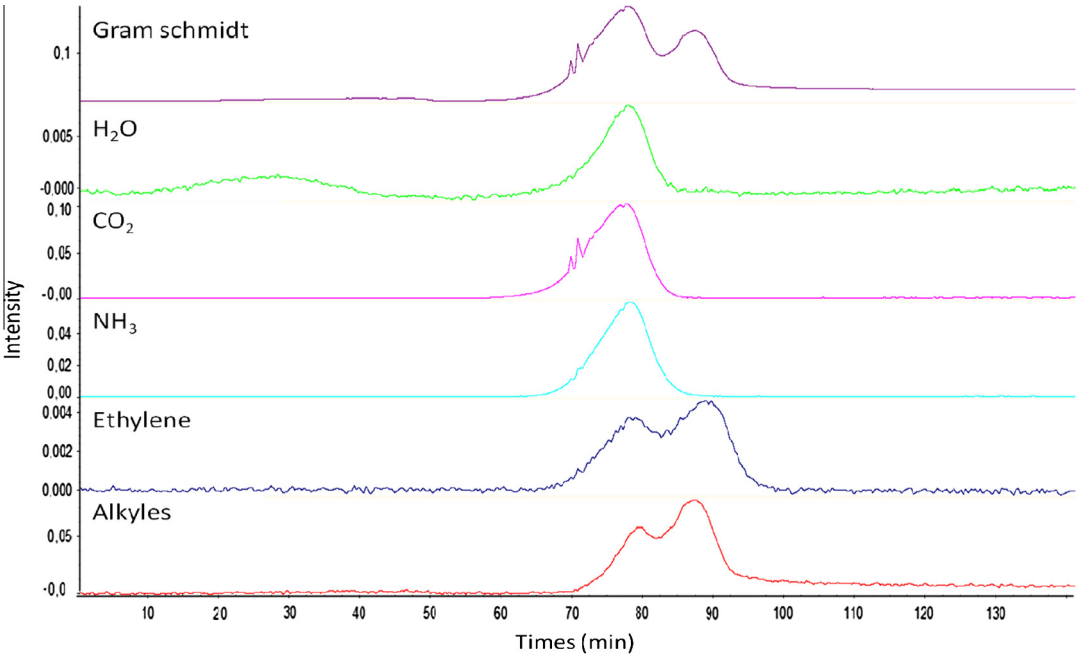

Fig. 9. Gram-Schmidt and chemigrams of C10SiDOPO under nitrogen.

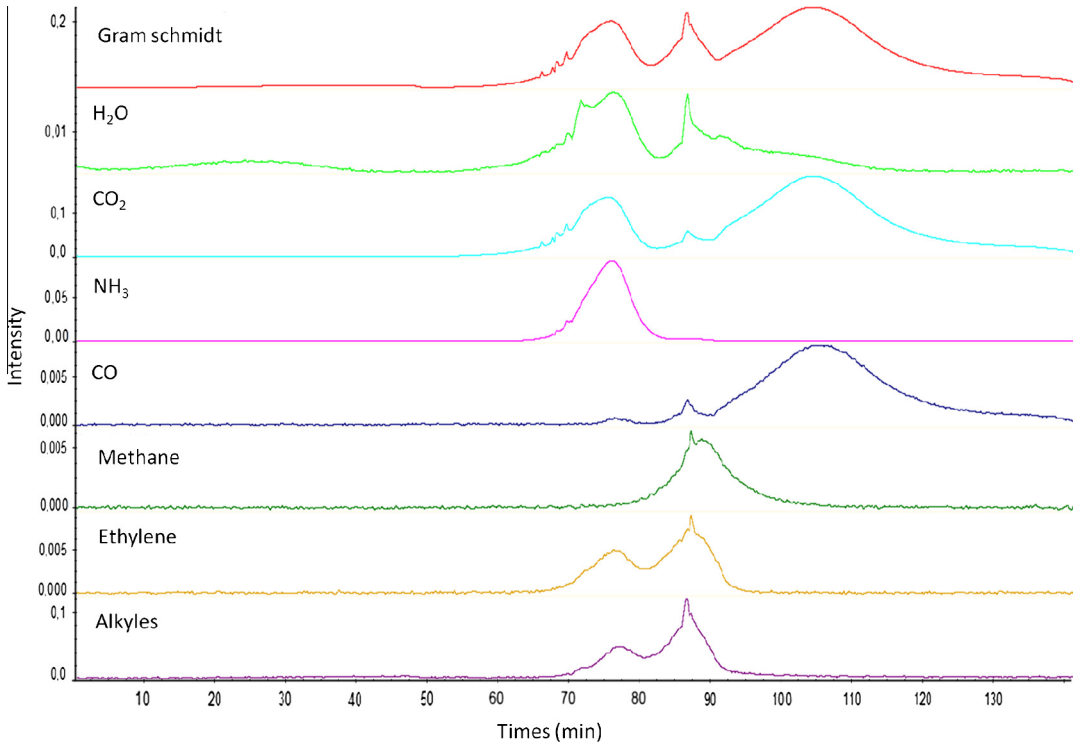

Fig. 10. Gram-Schmidt and chemigrams of C10SiDOPO under air.

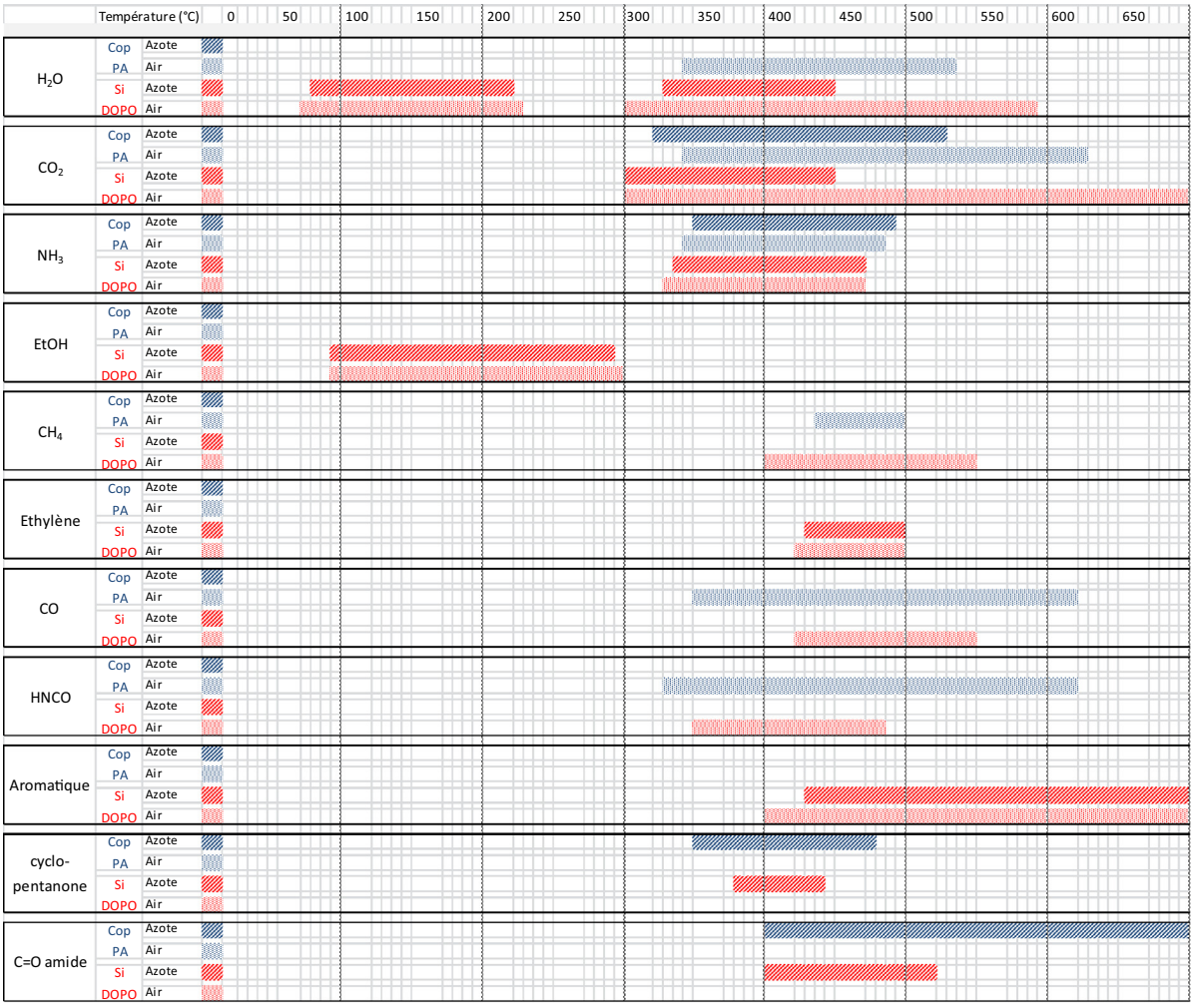

Fig. 11. Infrared table representing the different detected gases for Cop-PA and C10SiDOPO under air and nitrogen.

Si—O—Si vibrations. Another two bands were observed at 3074 and 1477 cm^{-1} corresponding to biphenyl and P-biphenyl respectively [34]. These observations indicate that there are phosphates and its derivatives in the gaseous phase.

3.6. Flammability and fire behavior

3.6.1. PCFC data

The HRC describes the potential of a material to release heat while burning, and is considered as a key parameter in determining the fire reaction of materials tested by PCFC, as it has been sometimes found to be proportional to the flaming HRR measured by conventional cone calorimeters [35]. Table 4 shows some results obtained from the PCFC. The Cop-PA is a highly flammable material which has a high peak of HRR and THR values. With the addition of 0.65 wt.% of Si and 0.75 wt.% of P, the peak of HRR (W/g) is decreased by around 24%. The THR (kJ/g) was also decreased about 6.3% with the addition of SiDOPO.

Table 4
PCFC results and combustion parameters from the cone calorimeter for the neat Cop-PA and C10SiDOPO.

Sample	Cop-PA	C10SiDOPO
PHRR (W/g)	618	468
TPHRR (°C)	458	443
THR (kJ/g)	26.9	25.2
HRC (J/g K)	592	468
TTI[a] (s)	77	62
PHRR[a] (kW/m^2)	886	597
THR[a] (MJ/m^2)	140.1	104.8
EHC[a] (kJ/g)	29.57	24.39
Residue[a] (wt.%)	0.63	5.98

[a] Cone calorimeter data.

As discussed before, the small peak around 200 °C (Fig. 12) was probably due to the ethanol released due to further hydrolysis–condensation reactions or trapped in the polymer matrix.

The reduction of HRC upon addition of SiDOPO could not be due to a dilution effect caused by the reduction of

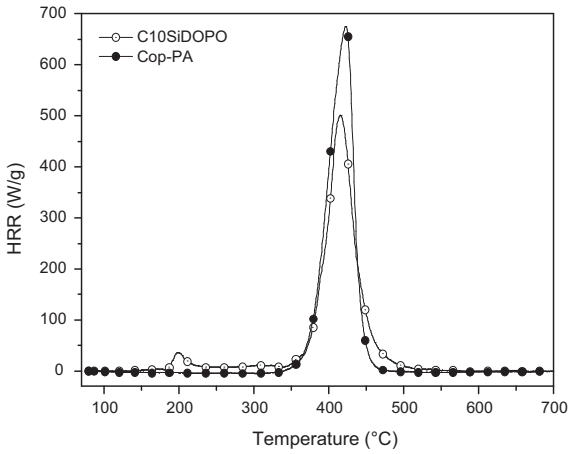

Fig. 12. PCFC curves for pure Cop-PA and C10SiDOPO composite versus the temperature of pyrolysis under nitrogen.

the amount of polymer as a consequence of the presence of the alkoxysilane precursor. These observations allow us to conclude that a significant reduction of fire hazards is caused by the presence of the SiDOPO. Since the degradation temperatures did not significantly change, thereby the expected value of PHRR in the cone calorimeter could be equal or even lower to the one obtained in PCFC [36].

3.6.2. Cone calorimeter data

The heat release rate curves as a function of time for the Cop-PA and SiDOPO based composite are presented in Fig. 13. The cone results measured at 50 kW/m^2 are summarized in Table 4.

The PA66 copolymer was characterized by an intense peak of heat release rate (PHRR) at 886 kW/m^2. The total heat release (THR) and the effective heat of combustion (EHC) were about 140 MJ/m^2 and 29.6 kJ/g respectively. As seen from HRR curve, its burning behavior is characteristic of an "intermediate thick non charring material" [37]. The sample was completely burned, leaving behind only a few residue.

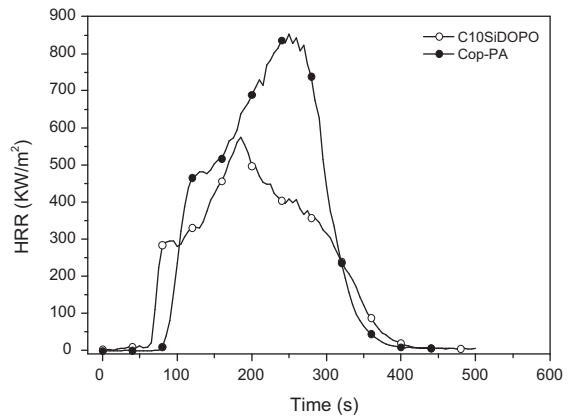

Fig. 13. HRR curves for pure Cop-PA and C10SiDOPO composite versus time at 50 kW/m^2.

With the SiDOPO nanocomposite, the ignition occurred a little bit earlier than that of Cop-PA. This faster ignition can probably be attributed to the catalytic effect of the phosphorous compounds and the release of ethanol before the ignition of the material. The PHRR was reduced by around 33% to values of about 597 kW/m^2. The THR decreased also around 25%. A decrease in the EHC value (around 18%) was also observed when SiDOPO was incorporated into the Cop-PA, suggesting an inhibition effect of the flame. Finally, the quantity of residue was increased of around 5%.

The materials showed also very different burning behaviors, especially with respect to the formation of a surface layer.

In fact, the shape of HRR curve for C10SiDOPO after the ignition of the material showed that the first peak of HRR was obtained at lower values than that of the neat copolymer. At the same time, a charred layer was formed, covering the surface of the sample. After a while, as more gases started to be released, a part of the layer expanded enormously (Fig. 14) in the center of the sample with the appearance of the second peak HRR. This second PHRR means that the layer is not very protective. This suggests that either the rate of phosphorus in the residue is not so sufficient to form a well protective barrier layer, or the structure of the layer requires the addition of other additives (for example inorganic FR) to increase its cohesion at the moment of the appearance of the second peak HRR during the test.

Fig. 14 shows the residues pictures of Cop-PA (a) and C10SiDOPO (b–d) after the cone calorimeter test. It was deduced that the Cop-PA forms a little residue. However, with the incorporation of 10 wt.% of SiDOPO, the appearance of a charred layer was observed. The pictures also revealed the presence of very expanded areas in the charred layer. Such behavior was also observed when 5 wt.% of condensed DOPO–VTES [P(DOPO–VTES)] and 2 wt.% of montmorillonite (MMT) were added in a polycarbonate matrix [17].

In order to show if the charred layer formed on the surface of the material is well cohesive, a microstructural analysis of C10SiDOPO residue by SEM was conducted.

3.6.2.1. Residue morphology. The morphology of the residue C10SiDOPO is shown in Fig. 15. At 1 mm, the charred layer presents a cohesive structure. At larger magnification (2 μm), the residue consists of very small spherical elementary particles, well agglomerated, forming a dense and cohesive network. These observations allow us to conclude that the charred layer obtained in the cone calorimeter test is relatively well cohesive.

3.6.2.2. Effective heat of combustion and combustion efficiency. Elemental analyzes of C10SiDOPO residue obtained from the cone calorimeter test are shown in Table 5. As the results show, for similar introduced quantities of silicon and phosphorus (ratio P/Si = 1.15), Si content is three times higher than P content in the residue (ratio = 0.32). Thus the phosphorus in SiDOPO is partially evolved as decomposition gases during combustion with a possible flame retardant action in the vapor phase.

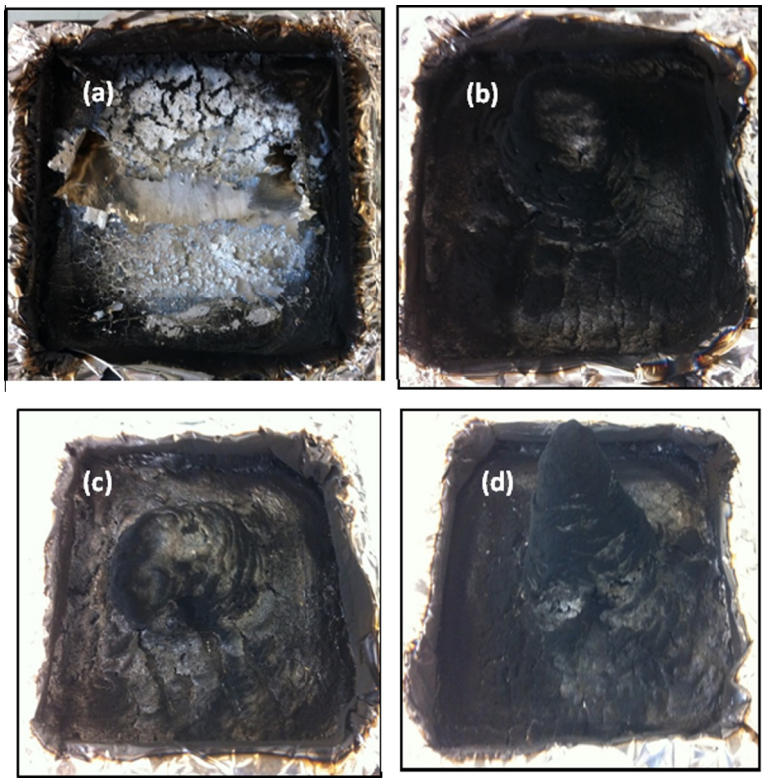

Fig. 14. Pictures of the residues obtained in the cone calorimeter for Cop-PA (a) and C10SiDOPO (b–d).

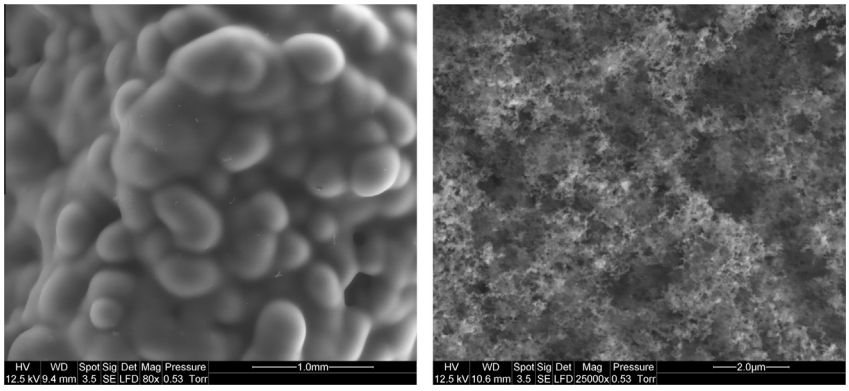

Fig. 15. SEM photographs of the residue C10SiDOPO.

Table 5
Data from elemental analysis for samples before and after cone calorimeter test.

Sample	P/Si sample	P/Si residue	Calculated% of Si[a]	Calculated% of P[a]	Residue (wt.%)
C10SiDOPO	1.15	0.32	0.93	0.30	5.98

[a] Elemental wt.% based on the weight of the residue in the cone calorimeter test.

Moreover it can be concluded that SiDOPO produces a double effect in the condensed phase: on one side a fraction of phosphorus promotes charring and on the other side silicon participates to the formation of a stable and cohesive residue.

With the aim to determine the action of SiDOPO in the vapor phase, effective heat of combustion was calculated. The release of phosphorous species may affect EHC by two ways: (i) it could reduce the combustion efficiency (χ) due to flame inhibition effect and (ii) their complete

Table 6
Combustion efficiency data.

Sample	THR_{PCFC} (kJ/g)	ML_{TGA}	EHC_{PCFC} (kJ/g)	EHC_{CC} (MJ/kg)	χ
Cop-PA	26.9	0.98	27.5	29.6	1.06
C10SiDOPO	25.2	0.92	27.3	24.4	0.89

combustion may release less heat than that of polymer degradation products [38].

In order to understand if the phosphorous compounds released into the gas phase have an influence as flame inhibitors, the combustion efficiency (χ) was calculated from the equation below:

$$\chi = \frac{EHC_{CC}}{EHC_{PCFC}} = \frac{EHC_{CC}}{THR_{PCFC}/ML_{TGA}} \quad (1)$$

where EHC_{CC} = effective heat of combustion from the cone calorimeter, EHC_{PCFC} = effective heat of complete combustion calculated from THR_{PCFC} = total heat release from the pyrolysis combustion flow calorimeter, and ML_{TGA} = mass loss from the TGA under Helium.

From the results shown in Table 6, and considering the measurement uncertainties, the combustion efficiency value for C10SiDOPO in the cone calorimeter is not close to 1, which means that the combustion is not totally complete. This proves that the decrease in EHC values is due to a flame inhibition effect due to the phosphorus released in the gas phase.

4. Conclusions

A new silicophosphorated precursor, SiDOPO, was successfully synthesized by addition reaction between vinyltriethoxysilane (VTES) and 9,10-dihydro-9-oxa-10-phosphaphenanthrene (DOPO). Hydrolysis–condensation reactions were performed in N-methylacetamide solvent with a low concentration of silica precursor and no addition of external catalyst. The hydrolyzed and condensed species and their evolution as a function of time were determined by ^{29}Si NMR spectroscopy. The inorganic precursor was then added into the PA66–PA6 matrix in the molten state at a constant flow rate. Composites showed a slightly lower onset decomposition temperature and a much higher amount of residue than the neat copolymer due to the good thermal stability of the SiDOPO. TGA-IR results showed that the addition of SiDOPO does not result in a significant change to the nature of decomposition gases. PCFC data showed a decrease by around 24% of the PHRR. Cone calorimeter results showed also a small decrease of the time to ignition and a reduction by around 33% of PHRR. The THR and the EHC were significantly decreased by 25% and 18% respectively. The change in fire behavior in the presence of SiDOPO was thought to be due to combined action of phosphorus and silicon in both the condensed and the vapor phase. In the condensed phase, phosphorus promotes the formation of a charred layer acting as barrier for gas and heat transfer, while silicon (as well as phosphorus) confers stability to this protective shield. In the gas phase, phosphorous species act as flame inhibitors as proved by the decrease of combustion efficiency and EHC values.

Acknowledgments

We thank the Region Rhône Alpes (France) and the University of Lyon (France) for financial support FUI SYRIMAP. Authors would like to thank Christine LUCAS for help in solid state NMR experiments, C2P2 (Chemistry, Catalysis, Polymer & Processes), UMR 5265 – University of Lyon 1.

References

[1] Pouxviel JC, Boilot JP, Beloeil JC, Lallemand JY. NMR study of the sol/gel polymerization. J Non-Crystall Solids 1987;89:345–60.
[2] Assink RA, Kay BD. Sol–gel kinetics I. Functional group kinetics. J Non-Crystall Solids 1988;99:359–70.
[3] Jang J, Park H. Formation and structure of polyacrylamide–silica nanocomposites by sol–gel process. J Appl Polym Sci 2002;83:1817–23.
[4] Hsiue GH, Liu YL, Liao HH. Flame-retardant epoxy resins: an approach from organic–inorganic hybrid nanocomposites. J Polym Sci Pol Chem 2001;39:986–96.
[5] Wang WJ, Perng LH, Hsiue GH, Chang FC. Characterization and properties of new silicone-containing epoxy resin. Polymer 2000;41:6113–22.
[6] Chiang C-L, Ma C-CM. Synthesis, characterization and thermal properties of novel epoxy containing silicon and phosphorus nanocomposites by sol–gel method. Eur Polym J 2002;38:2219–24.
[7] Alongi J, Colleoni C, Malucelli G, Rosace G. Hybrid phosphorus-doped silica architectures derived from a multistep sol–gel process for improving thermal stability and flame retardancy of cotton fabrics. Polym Degrad Stab 2012;97:1334–44.
[8] Theil-Van Nieuwenhuyse R, Bounor-Legare V, Bardollet P, Cassagnau P, Michel A, David L, et al. Phosphorylated silica/polyamide 6 nanocomposites synthesis by in situ sol–gel method in molten conditions: impact on the fire-retardancy. Polym Degrad Stab 2013;98:2635–44.
[9] Sahyoun J, Bounor-Legaré V, Ferry L, Sonnier R, Bonhommé A, Cassagnau P. Influence of organophosphorous silica precursor on the thermal and fire behaviour of a PA66/PA6 copolymer. Polym Degrad Stab 2015. http://dx.doi.org/10.1016/j.polymdegradstab.2015.02.017.
[10] Bonnet J, Bounor-Legare V, Boisson F, Melis F, Camino G, Cassagnau P. Phosphorus based organic–inorganic hybrid materials prepared by reactive processing for EVA fire retardancy. Polym Degrad Stab 2012;97:513–22.
[11] Zhong HF, Wei P, Jiang PK, Wang GL. Thermal degradation behaviors and flame retardancy of PC/ABS with novel silicon-containing flame retardant. Fire Mater 2007;31:411–23.
[12] Liu YL. Flame-retardant epoxy resins from novel phosphorus-containing novolac. Polymer 2001;42:3445–54.
[13] Rakotomalala M, Wagner S, Doring M. Recent developments in halogen free flame retardants for epoxy resins for electrical and electronic applications. Materials 2010;3:4300–27.
[14] Schartel B, Braun U, Balabanovich AI, Artner J, Ciesielski M, Doring M, et al. Pyrolysis and fire behaviour of epoxy systems containing a novel 9,10-dihydro-9-oxa-10-phosphaphenanthrene-10-oxide-(DOPO)-based diamino hardener. Eur Polym J 2008;44:704–15.
[15] Zhang WC, Yang RJ. Synthesis of phosphorus-containing polyhedral oligomeric silsesquioxanes via hydrolytic condensation of a modified silane. J Appl Polym Sci 2011;122:3383–9.
[16] Alongi J, Malucelli G. Cotton fabrics treated with novel oxidic phases acting as effective smoke suppressants. Carbohydr Polym 2012;90:251–60.
[17] Hu Z, Chen L, Zhao B, Luo YA, Wang DY, Wang YZ. A novel efficient halogen-free flame retardant system for polycarbonate. Polym Degrad Stab 2011;96:320–7.
[18] Wei P, Tian G, Yu H, Qian Y. Synthesis of a novel organic–inorganic hybrid mesoporous silica and its flame retardancy application in PC/ABS. Polym Degrad Stab 2013;98:1022–9.
[19] Qian XD, Song L, Hu Y, Yuen RKK. Thermal degradation and flammability of novel organic/inorganic epoxy hybrids containing organophosphorus-modified oligosiloxane. Thermochim Acta 2013;552:87–97.

[20] Albert K, Bayer E. Characterization of bonded phases by solid-state NMR-spectroscopy. J Chromatogr 1991;544:345–70.
[21] Huggett C. Estimation of rate of heat release by means of oxygen-consumption measurements. Fire Mater 1980;4:61–5.
[22] Schartel B, Pawlowski KH, Lyon RE. Pyrolysis combustion flow calorimeter: a tool to assess flame retarded PC/ABS materials? Thermochim Acta 2007;462:1–14.
[23] Wagner Sebastian, Rakotomalala Muriel, Chesneau Frederick, Zevaco Thomas, Döring M. Spectral assignment of phenanthrene derivatives based on 6H-Dibenzo[C, E][1,2] Oxaphosphinine 6-Oxide by NMR and quantum chemical calculations. Phosphorus Sulfur Silicon Related Elem 2012;187:781–98.
[24] Van Nieuwenhuyse P, Bounor-Legare V, Boisson F, Cassagnau P, Michel A. Hydrolysis–condensation reactions of diethylphosphato-ethyltriethoxysilane with tetraethoxysilane studied by Si-29-NMR: solvent and phosphonate catalytic effect. J Non-Crystall Solids 2008;354:1654–63.
[25] Cardenas A, Hovnanian N, Smaihi M. Sol–gel formation of heteropolysiloxanes from diethylphosphatoethyltriethoxysilane and tetraethoxysilane. J Appl Polym Sci 1996;60:2279–88.
[26] Dabrowski F, Bourbigot S, Delobel R, Le Bras M. Kinetic modelling of the thermal degradation: of polyamide-6 nanocomposite. Eur Polym J 2000;36:273–84.
[27] Braun U, Schartel B, Fichera MA, Jager C. Flame retardancy mechanisms of aluminium phosphinate in combination with melamine polyphosphate and zinc borate in glass-fibre reinforced polyamide 6,6. Polym Degrad Stab 2007;92:1528–45.
[28] Hornsby PR, Wang J, Rothon R, Jackson G, Wilkinson G, Cossick K. Thermal decomposition behaviour of polyamide fire-retardant compositions containing magnesium hydroxide filler. Polym Degrad Stab 1996;51:235–49.
[29] Schaffer MA, McAuley KB, Marchildon EK, Cunningham MF. Thermal degradation kinetics of nylon 66: experimental study and comparison with model predictions. Macromol React Eng 2007;1:563–77.
[30] Qian LJ, Ye LJ, Qiu Y, Qu SR. Thermal degradation behavior of the compound containing phosphaphenanthrene and phosphazene groups and its flame retardant mechanism on epoxy resin. Polymer 2011;52:5486–93.
[31] Perret B, Schartel B, Stoss K, Ciesielski M, Diederichs J, Doring M, et al. Novel DOPO-based flame retardants in high-performance carbon fibre epoxy composites for aviation. Eur Polym J 2011;47:1081–9.
[32] Wu ZJ, Li JL, Chen YP, Wang Z, Li SC. Effect of 9,10-dihydro-9-oxa-10-phosphaphenanthrene-10-oxide on liquid oxygen compatibility of bisphenol A epoxy resin. J Appl Polym Sci 2014;131.
[33] Bai ZM, Jiang SD, Tang G, Hu Y, Song L, Yuen RKK. Enhanced thermal properties and flame retardancy of unsaturated polyester-based hybrid materials containing phosphorus and silicon. Polym Adv Technol 2014;25:223–32.
[34] Zhang WC, Li XM, Guo XY, Yang RJ. Mechanical and thermal properties and flame retardancy of phosphorus-containing polyhedral oligomeric silsesquioxane (DOPO–POSS)/polycarbonate composites. Polym Degrad Stab 2010;95:2541–6.
[35] Lyon RE, Walters RN. Pyrolysis combustion flow calorimetry. J Anal Appl Pyrolysis 2004;71:27–46.
[36] Sonnier R, Ferry L, Longuet C, Laoutid F, Friederich B, Laachachi A, et al. Combining cone calorimeter and PCFC to determine the mode of action of flame-retardant additives. Polym Adv Technol 2011;22:1091–9.
[37] Schartel B, Weiss A. Temperature inside burning polymer specimens: pyrolysis zone and shielding. Fire Mater 2010;34:217–35.
[38] Sonnier R, Otazaghine B, Ferry L, Lopez-Cuesta J-M. Study of the combustion efficiency of polymers using a pyrolysis–combustion flow calorimeter. Combust Flame 2013;160:2182–93.